Metabolism 151 (2024) 155746

Contents lists available at ScienceDirect

Metabolism

journal homepage: www.journals.elsevier.com/metabolism

Tm4sf19 deficiency inhibits osteoclast multinucleation and prevents bone loss

Sujin Park [a,1], Jin Sun Heo [a,1], Seiya Mizuno [b,1], Minwoo Kim [c,d,1], Haein An [a,e,1], Eunji Hong [a,e,1], Min Gi Kang [a,e], Junil Kim [f], Rebecca Yun [a,g], Hyeyeon Park [a,e], Eun Hye Noh [c], Min Jung Lee [c], Kwiyeom Yoon [c], Pyunggang Kim [a], Minjung Son [a,e], Kyoungwha Pang [a], Jihee Lee [a], Jinah Park [a,h], Akira Ooshima [a], Tae-Jin Kim [i], Je Yeon Park [a], Kyung-Min Yang [c], Seung-Jae Myung [j], Hyun Bae [k], Kyung-Mi Lee [l], John Letterio [m,n], Seok Hee Park [e], Satoru Takahashi [o], Seong-Jin Kim [a,c,*]

[a] GILO Institute, GILO Foundation, Seoul, Republic of Korea
[b] Laboratory Animal Resource Center in Transborder Medical Research Center, Institute of Medicine, University of Tsukuba, Tsukuba, Japan
[c] Medpacto Inc., Seoul, Republic of Korea
[d] Department of Biochemistry, College of Life Science & Biotechnology, Yonsei University, Seoul, Republic of Korea
[e] Department of Biological Sciences, Sungkyunkwan University, Suwon, Republic of Korea
[f] School of Systems Biomedical Science, Soongsil University, Seoul, Republic of Korea
[g] Cancer Research Institute, Seoul National University College of Medicine, Seoul, Republic of Korea
[h] Amoris Bio Inc., Seoul, Republic of Korea
[i] Division of Radiation Biomedical Research, Korea Institute of Radiological & Medical Sciences, Seoul, Republic of Korea
[j] Department of Gastroenterology, University of Ulsan College of Medicine, Asan Medical Center, Seoul, Republic of Korea
[k] Cedars-Sinai Medical Center, Los Angeles, CA, USA
[l] Department of Biochemistry and Molecular Biology, College of Medicine, Korea University, Seoul, Republic of Korea
[m] Case Comprehensive Cancer Center, Case Western Reserve University and Department of Pediatrics, Case Western Reserve University School of Medicine, Cleveland, OH, USA
[n] The Angie Fowler Adolescent & Young Adult Cancer Institute, University Hospitals Rainbow Babies & Children's Hospital, Cleveland, OH, USA
[o] Department of Anatomy and Embryology, Faculty of Medicine, University of Tsukuba, Tsukuba, Japan

ARTICLE INFO

Keywords:
Bone
Tm4sf19
Integrin αvβ3
Osteoclast
Osteoporosis

ABSTRACT

Background: Multinucleation is a hallmark of osteoclast formation and has a unique ability to resorb bone matrix. During osteoclast differentiation, the cytoskeleton reorganization results in the generation of actin belts and eventual bone resorption. Tetraspanins are involved in adhesion, migration and fusion in various cells. However, its function in osteoclast is still unclear. In this study, we identified Tm4sf19, a member of the tetraspanin family, as a regulator of osteoclast function.

Materials and methods: We investigate the effect of Tm4sf19 deficiency on osteoclast differentiation using bone marrow-derived macrophages obtained from wild type (WT), Tm4sf19 knockout (KO) and Tm4sf19 LELΔ mice lacking the large extracellular loop (LEL). We analyzed bone mass of young and aged WT, KO and LELΔ mice by μCT analysis. The effects of Tm4sf19 LEL-Fc fusion protein were accessed in osteoclast differentiation and osteoporosis animal model.

Results: We found that deficiency of Tm4sf19 inhibited osteoclast function and LEL of Tm4sf19 was responsible for its function in osteoclasts *in vitro*. KO and LELΔ mice exhibited higher trabecular bone mass compared to WT mice. We found that Tm4sf19 interacts with integrin αvβ3 through LEL, and that this binding is important for cytoskeletal rearrangements in osteoclast by regulating signaling downstream of integrin αvβ3. Treatment with LEL-Fc fusion protein inhibited osteoclast function *in vitro* and administration of LEL-Fc prevented bone loss in an osteoporosis mouse model *in vivo*.

* Corresponding author at: GILO Institute, GILO Foundation, 92 Myeongdal-ro, Seocho-gu, Seoul 06668, Republic of Korea.
E-mail address: jasonsjkim@gilo.or.kr (S.-J. Kim).

[1] Sujin Park, Jin Sun Heo, Seiya Mizuno, Minwoo Kim, Haein An, and Eunji Hong contributed equally.

https://doi.org/10.1016/j.metabol.2023.155746
Received 15 September 2023; Accepted 23 November 2023
Available online 26 November 2023
0026-0495/© 2023 The Authors. Published by Elsevier Inc. This is an open access article under the CC BY-NC-ND license (http://creativecommons.org/licenses/by-nc-nd/4.0/).

Conclusion: We suggest that Tm4sf19 regulates osteoclast function and that LEL-Fc may be a promising drug to target bone destructive diseases caused by osteoclast hyper-differentiation.

Abbreviation

Tm4sf19	Transmembrane 4 L6 family member 19
LEL	the large extracellular loop
OCTM4	osteoclast maturation-associated gene 4 protein
RANKL	receptor activator of nuclear factor kB ligand
M-CSF	macrophage colony-stimulating factor
BMMs	bone marrow-derived macrophages
TEMs	tetraspanin-rich microdomains
TRAcP 5b	Tartrate-resistant acid phosphatase 5b
μCT	micro-computed tomography
BMD	bone mineral density
BV/TV	bone volume/tissue volume
Tb.Sp.	trabecular separation
Tb.N.	trabecular number
DEGs	differentially expressed genes

1. Introduction

Osteoclast and osteoblast cooperate to maintain bone homeostasis [1]. Osteoclasts derived from hematopoietic stem cells differentiate into multinucleated cells, which are essential processes for bone resorption by RANKL (receptor activator of nuclear factor kB ligand) and M-CSF (macrophage colony-stimulating factor) [2–4]. Osteoclast multinucleation occurs by intercellular fusion through reorganization of the cytoskeleton. During osteoclast differentiation, mononuclear progenitor cells undergo cytoskeletal rearrangements to attach to the bone surface, form multinucleated cells, and then efficiently resorb bone. This process is controlled by a complex network of signaling pathways, and disruption of these pathways results in various bone diseases such as osteopetrosis and osteoporosis [5].

Tetraspanins, also known as the transmembrane superfamily (TM4SFs), are a family of transmembrane proteins with four alpha-helical transmembrane domains and two extracellular domains. Proteins of the tetraspanin family are involved in proliferation, differentiation, apoptosis, adhesion, migration and signal transduction in various cells, and also play an essential role in cell-cell fusion [6]. Of the 33 tetraspanin members in humans, several tetraspanins have been reported to be required for osteoclast function [7–9]. Transmembrane 4 L6 family member 19 (Tm4sf19) is a member of the tetraspanin family, and it is also known as OCTM4 (osteoclast maturation-associated gene 4 protein. There are few reports demonstrated the expression of Tm4sf19 was increased in inflammation, however the role of Tm4sf19 in osteoclast maturation is still unclear [10]. The expression of Tm4sf19 is very low in most tissues compared to osteoclasts (Fig. S1).

In this study, we identified Tm4sf19 as a regulator of osteoclast differentiation. The expression of Tm4sf19 was increased in a later stage of osteoclast differentiation. We found that the osteoclast function was impaired in bone marrow-derived macrophages (BMMs) obtained from Tm4sf19 KO and LELΔ mice. We also found that systemic knockout mice of Tm4sf19 have higher bone mass due to inhibition of osteoclast function, and that the LEL of Tm4sf19 is important for its function and its binding to integrin αvβ3. In addition, it was confirmed that the LEL-Fc fusion protein effectively inhibits osteoclast function and bone resorption activity by impairing cytoskeletal rearrangement *in vitro* and has therapeutic effect of osteoporosis-induced bone destruction *in vivo*. Our findings suggest that Tm4sf19 is a potential therapeutic target to inhibit osteoclast function and bone resorption. We also demonstrated that the Tm4sf19 LEL-Fc fusion protein has a therapeutic effect on ovariectomy-induced bone loss.

2. Materials and methods

2.1. Mice

All animal experiments procedures approved by the Institutional Animal Care and Use Committee (IACUC) of Medpacto (Approval No. 2021-0009) and performed following the ARRIVE 2.0 guidelines.

2.2. Preparation of mouse bone marrow cells

Tibias and femurs were separated from 6 to 8-week-old mice. To obtain the bone marrow, the bones were flushed with DMEM (High glucose, WelGENE Inc., Daegu, Korea) culture media using a 23-gauge needle. Bone marrow cells were collected, washed with PBS, pelleted, and resuspended in α-MEM (Gibco, 41061029) supplemented with 10 % FBS, penicillin-streptomycin (WelGENE Inc.) and amphotericin B mixture (GenDEPOT, CA002-010) and stimulated with 5 ng/ml M-CSF (PEPROTECH, 315-02). After overnight incubation, non-adherent cells were collected and re-suspended in complete α-MEM, containing 30 ng/mL human recombinant M-CSF for 3 days. Adherent bone marrow derived macrophages (BMMs) were washed twice with PBS and cultured with M-CSF and RANKL to differentiate into pre-osteoclasts (pre-OCs) or mature osteoclasts. The culture media were replaced every two days. Vitronectin (Advanced biomatrix, 5051) was coated on plate according to described methods with manufacturer.

2.3. Immunofluorescence

Cells were seeded on confocal plate and incubated in indicated culture media. Cells were washed with PBS and fixed in 4 % paraformaldehyde in PBS for 5 min. Then cells were incubated in PBS containing 3 % FBS for 1 h. After overnight incubation at 4 °C with appropriate primary antibodies, cells were washed with PBS and incubated with Alexa Flour conjugated secondary antibodies). For the F-actin detection, cells were stained using Phalloidin-I Fluor 488 for 20 min in room temperature. Nuclei were counterstained with DAPI (Sigma-Aldrich).

2.4. TRAP staining

Cells were washed with 1× PBS once, then fixed with 10 % neutral-buffered formalin for 5 min and washed with distilled water twice. Cells were incubated at 37 °C for 20 min with the tartrate-resistant acid phosphatase (TRAP) activity kit according to the manufacturer's instructions (COSMO BIO) and washed once with distilled water.

2.5. Microcomputed tomography (μCT) analysis

Murine femurs and tibias were fixed in 10 % neutral-buffered formalin and scanned by micro-computed tomography (Skyscan 1172) under 50 kV, 200 μA, 600 ms condition. Scan data was three-dimensionally reconstructed using NRecon software. Bone mineral density and trabecular morphometry were obtained using CTAn software. The trabecular structures were selected 2 mm from growth plate. Data was visualized using CTvox software.

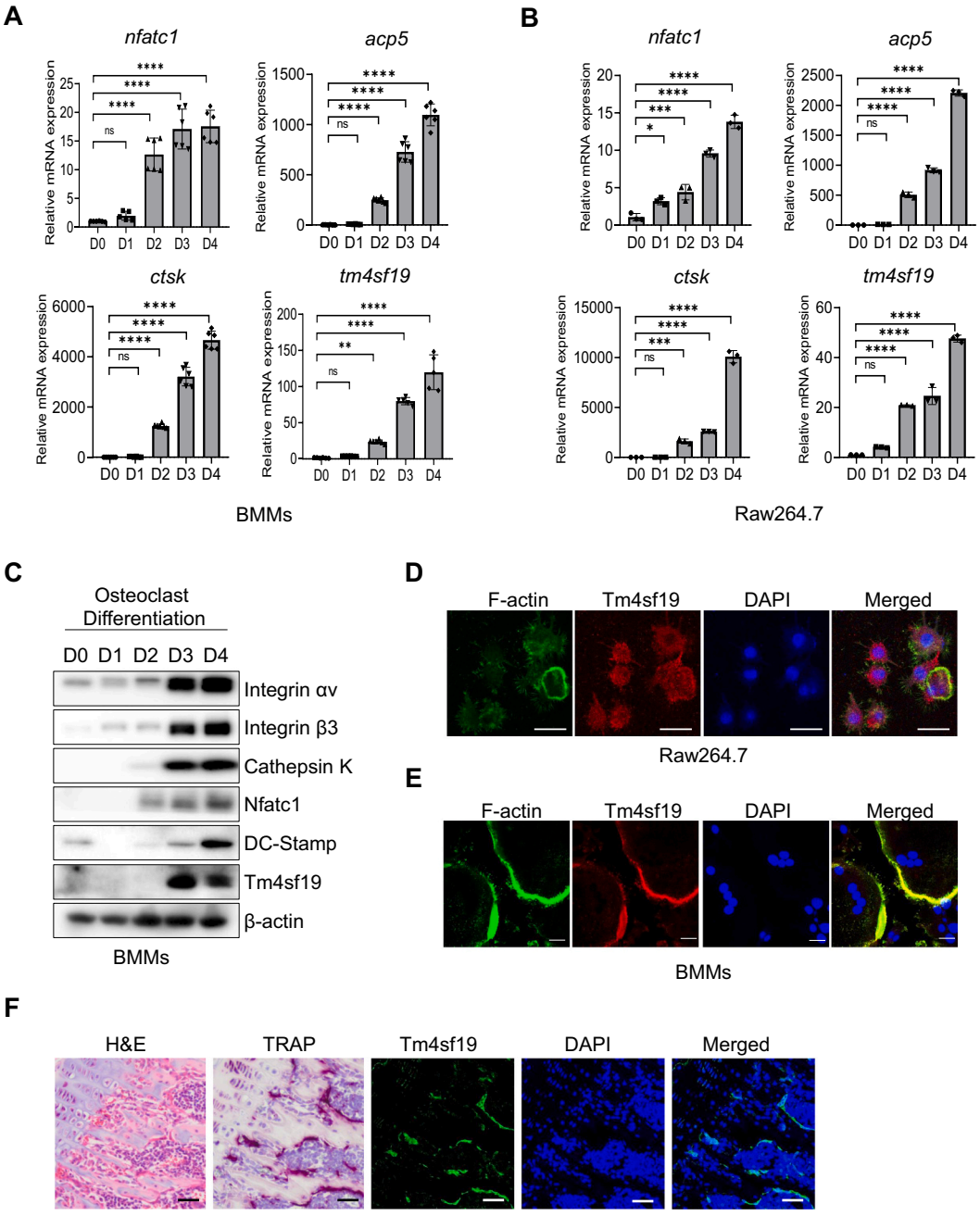

Fig. 1. Depletion of *tm4sf19* impairs osteoclast differentiation. (A–B) Expression of *tm4sf19* and osteoclast differentiation markers during osteoclastogenesis. qPCR analysis of *nfatc1*, *acp5*, *ctsk* and *tm4sf19* on day 0–4 in (A) BMMs and (B) Raw264.7 cells. Statistical analysis was performed in at least three replicates. (C) Immunoblot analysis of Tm4sf19 and osteoclast-specific proteins. β-actin was used as a loading control. (D) Representative image of F-actin (green) and Tm4sf19 (red) labeled osteoclasts. Raw264.7 cells stably expressed Tm4sf19 was cultured under RANKL stimulation and fixed at the early time of osteoclast differentiation. The single nucleus (DAPI) presents mononucleated osteoclast. Scale bars; 20 μm. (E) Representative confocal microscopy images of multinucleated osteoclasts plated on a fibronectin-coated plates. Co-localization of Tm4sf19 and F-actin on the actin belt in the extracellular matrix was visualized. DAPI was used for nuclear DNA staining. Scale bar, 20 μm. (F) H&E, TRAP and immunofluorescence staining images of Tm4sf19 on the tibia of WT mice. Scale bar, 100 μm. All quantitative analyzes to show significance were calculated by one-way ANOVA; $^{**}p < 0.01$, $^{***}p < 0.001$, $^{****}p < 0.0001$, ns = no significant.

2.6. Ovariectomy-induced osteoporosis (OVX) model

8-Week-old female C57BL/6J mice were subjected to sham or ovariectomy surgery. Both ovaries were removed in ovariectomized mice and skin incision was preceded in sham group. For Fc fusion treatment experiments, the ovariectomized mice were randomly assigned to 3 groups and administrated with mock or 5, or 10 mpk LEL-Fc in intravenously injection once a week for 4 weeks started at two days after surgery. Both tibia and femur were collected for histological analysis and μCT analysis.

2.7. Statistics

Data are shown as the mean ± SD. The number of samples and replications were described in the figure legends. The significance of data was determined by two-tailed or unpaired *t*-tests, one-way ANOVA and two-way ANOVA. *P* values are presented on the graphs as *<0.05, **<0.01, ***<0.001, and ****≤0.0001. GraphPad Prism 8 software was

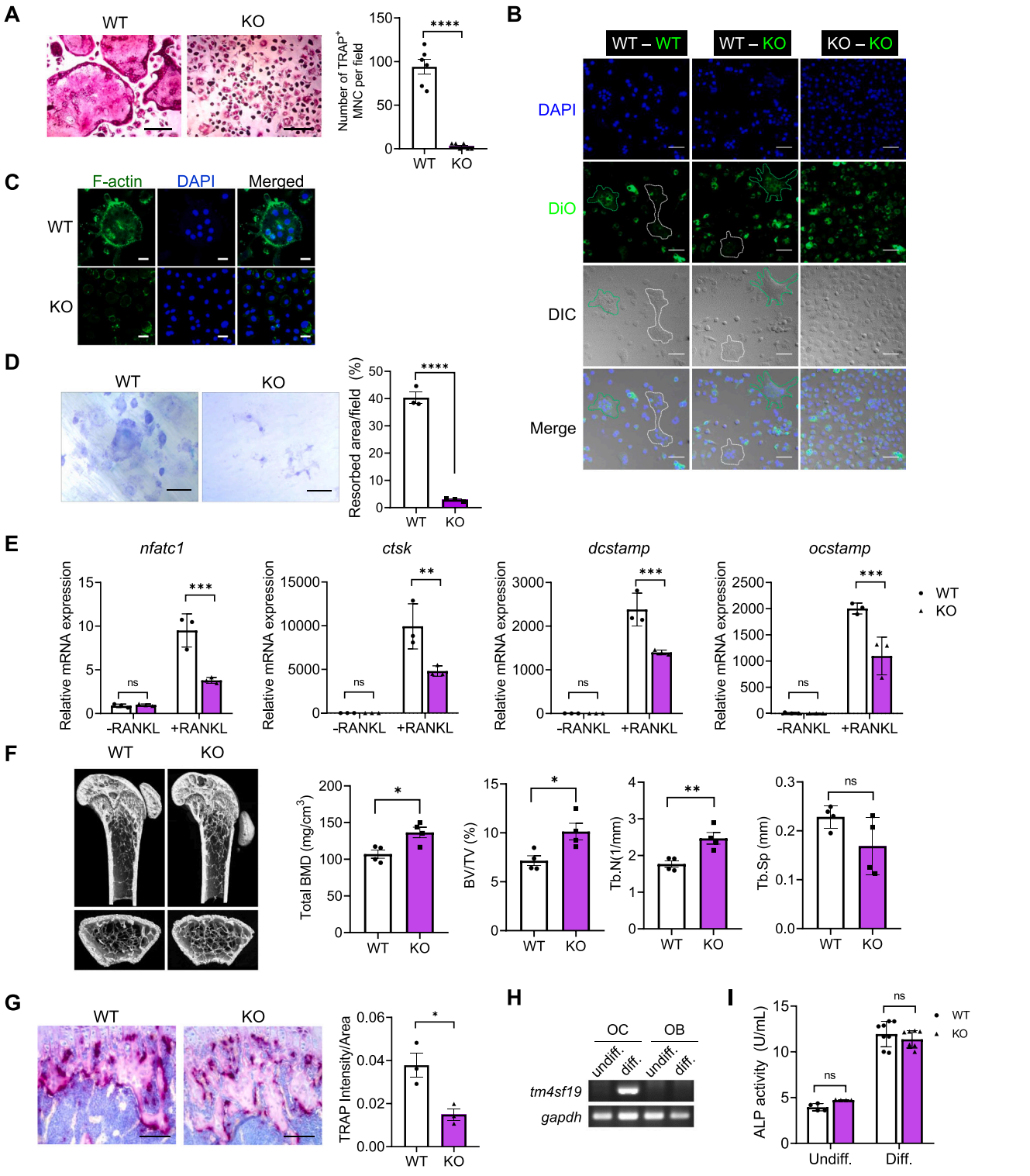

(caption on next page)

Fig. 2. Effect of *tm4sf19* deficiency impaired osteoclast function. (A) Representative TRAP staining images and measurement of TRAP-positive cells of *tm4sf19*$^{+/+}$ (WT) and *tm4sf19*$^{-/-}$ (KO) osteoclast differentiation. Scale bar, 200 μm. (B) DiO-(green)-labeled follower and unlabeled founder osteoclasts were mixed and differentiated for multinucleation. Both WT-WT and WT-KO mixtures show fluorescence-positive (green dotted line) and negative (white dotted line) multinucleated osteoclasts. DAPI represents the nuclei numbers and DIC represents the bright image of the cell. Scale bars; 50 μm. (C) Confocal microscopy images of actin rings and actin belt (F-actin) in WT and KO osteoclasts after osteoclast differentiation. Scale bar, 20 μm. (D) Bone resorption pit assay using mature WT and KO osteoclasts using dentine discs. Blue stained structures indicate resorption pits. Scale bars; 50 μm. Resorbed area per field was analyzed. (E) Relative mRNA expression of osteoclast differentiation and fusion marker genes. (F) Micro-computed tomography (μCT) analysis of the femur obtained from 3-month-old WT and KO female mice. Representative 3D images of distal femoral trabecular region from WT and KO mice. Trabecular bone was specified at a height of 2 mm from the growth plate. Total bone mineral density (BMD), bone volume/tissue volume (BV/TV), trabecular number (Tb.N) and separation of trabecular (Tb.Sp) were analyzed. (G) Representative images of TRAP staining of the femurs of WT and KO mice. Scale bar, 100 μm. Relative TRAP intensities per area were analyzed. (H-K) Osteoblasts were isolated from 2- to 3-day-old calvaria of WT and KO mice and differentiated with or without osteogenic induction for 21 days. (H) The expression of *tm4sf19* in undifferentiated or differentiated osteoclast and osteoblast. (I) ALP activity was measured on differentiated osteoblast compared to undifferentiated osteoblast precursor from WT and KO mice. (J) Representative images of Alizarin red staining of differentiated osteoblasts. Relative absorbance of each well was calculated comparing WT and KO. (K) Relative mRNA expression of osteoblast differentiation-related genes. All quantitative analyzes to show significance were calculated by *t*-test or two-way ANOVA; $*p < 0.05$, $**p < 0.01$, $***p < 0.001$, $****p < 0.0001$, ns = no significant.

used for statistical analysis and generation of graphs.

3. Results

3.1. The expression of tm4sf19 is markedly increased in later stages of osteoclast differentiation and tm4sf19 mainly expressed in the actin belt of mature osteoclast

It is known that RANKL increases the expression of various osteoclast-specific genes, including *nfatc1*, *acp5*, *ctsk*, *itgav*, *itgb3*, and *dcstamp* during osteoclast differentiation [11]. We found that the expression of the *tm4sf19* gene is significantly increased at a late phase of osteoclast differentiation (Figs. 1A–B, and S2A–B). The expression of Tm4sf19 protein and various osteoclast-associated proteins also increases significantly during osteoclast differentiation (Figs. 1C and S2C). Rearrangement of the actin cytoskeleton and the formation of actin rings and actin belts also occur during osteoclast differentiation [2,12–15]. We examined the localization of Tm4sf19 using Tm4sf19 stably expressing Raw 264.7 cells under RANKL stimulation. Tm4sf19 was localized not only to the actin ring, but also to the filopodia, the stretched structures for searching cells to fuse, and the fusopod, the cytoplasmic bridge for contacting other osteoclasts to fuse (Fig. 1D). In multinucleated osteoclasts, Tm4sf19 was mainly expressed in the actin belt of mature osteoclasts and co-localized with F-actin (Fig. 1E). In addition, we found Tm4sf19 protein expression in osteoclasts of mouse trabecular bone region as confirmed by H&E and TRAP staining in sequential sections (Fig. 1F). These data suggest that Tm4sf19 may involve in osteoclast function.

3.2. Tm4sf19 deficiency inhibited osteoclast function

We found that Tm4sf19 is mainly expressed in osteoclast (Fig. S1). To determine the role of Tm4sf19 in osteoclastogenesis, we generated a CRISPR-based systemic Tm4sf19 knockout (*tm4sf19*$^{-/-}$, KO) mouse (Fig. S3) [16]. KO mice were born at the Mendelian rate and had no distinct phenotype. We performed *in vitro* cultures of osteoclasts generated from BMMs derived from *tm4sf19*$^{+/+}$ (WT), and KO mice in the presence of M-CSF and RANKL. Surprisingly, osteoclast multinucleation was inhibited in osteoclasts derived from KO mouse BMMs despite the presence of TRAP-positive mononuclear cells observed (Figs. 2A and S4A). When the concentration of M-CSF was increased to 100 ng/ml, osteoclast differentiation was enhanced in WT osteoclasts, but KO osteoclasts still failed to form multinucleated osteoclasts. (Fig. S4B). Next, the formation of multinucleated osteoclasts was examined by time-lapse microscope using DiO (green)-stained progenitor cells (founder cells grown in osteoclastic differentiation media), and DiL (red)-stained follower cells grown in growth media supplemented with M-CSF only [17–19]. We found multinucleated osteoclasts formation when both the founder and follower cells were WT cells, but it was suppressed when both the founder and follower cells were KO cells (Fig. S4C and Supplementary Movies 1, 2). To investigate whether Tm4s19 is required for multinucleated osteoclast formation, DiO (green)-labeled follower cells were co-cultured with unlabeled founder cells. Multinucleated osteoclast formation was found in mixed cultures of WT-founder and WT-follower and mixed cultures of WT-founder and KO-follower cells, but not in mixed cultures of KO-founder and KO-follower cells (Fig. 2B). These results suggest that the expression of tm4sf19 in osteoclasts is important for the formation of multinucleated osteoclasts. Based on the finding that Tm4sf19 localizes to the actin belt after osteoclast maturation, we investigated whether Tm4sf19 is involved in cytoskeletal rearrangements leading to bone resorption activity. During osteoclast differentiation, cytoskeleton rearrangement and formation of actin rings and actin belts were observed in WT osteoclasts, whereas KO osteoclasts formed actin rings but did not form actin belts (Fig. 2C). We also found that bone resorption activity was significantly reduced in KO osteoclasts (Fig. 2D). Next, we confirmed that the expression of osteoclast differentiation-related markers, *nfatc1* and *ctsk*, and osteoclast fusion markers, *dcstamp* and *ocstamp* were reduced after osteoclast differentiation in KO osteoclasts compared to WT osteoclasts (Fig. 2E).

Next, we confirmed the Tm4sf19 protein expression on osteoclasts in the tibia of WT mice, but not in KO mice (Fig. S5). Because bone resorption activity was significantly inhibited in KO osteoclasts, it is likely that trabecular bone mass was increased in KO mice, therefore we analyzed changes in trabecular bone in 3-month-old female WT and KO mice by μCT analysis. As we expected, total BMD, BV/TV ratio and Tb.N of the femur was significantly higher and Tb.Sp was lower in KO mice compared to WT mice (Fig. 2F). Bone density in mouse peaks at 5 to 6 months, and skeletal aging occurs at around 18 months. Therefore, we analyzed skeletal changes in young (6–7 months old) and aged (17–18 months old) male WT and KO mice. In WT mice, total BMD of the femur and lumbar spine gradually decreased over time, whereas the decrease was not observed in KO mice. BV/TV ratio of femur and Tb.Sp of lumbar was more pronounced with age in WT mice compared to KO mice (Fig. S6A–B). Unexpectedly, serum TRAcP 5b, which reflects osteoclast numbers, showed little difference when comparing serum levels in WT mice with serum levels in KO mice (Fig. S6C). BMMs from KO mice were able to form TRAP-positive mononuclear osteoclasts *in vitro*, but the formation of multinucleated osteoclasts was inhibited (Figs. 2A–B and S4A–C). These data indicate that Tm4sf19 deficiency does not affect osteoclast number but only affects osteoclast multinucleation. However, we cannot rule out the possibility that there are dysfunctional osteoclasts that do not form multinucleated osteoclasts and are not resorbed on the bone surface. Histological analysis revealed increased trabecular bone mass and decreased osteoclast activity by TRAP staining of the trabecular surface in KO mice compared to WT mice, suggesting that osteoclast differentiation may be inhibited in KO mice (Fig. 2G). However, no or little differences were found in epiphyseal cartilage of WT and Tm4sf19 KO mice confirmed by Alcian blue staining (Fig. S6D).

Next, we investigated whether Tm4sf19 is also involved in osteoblast

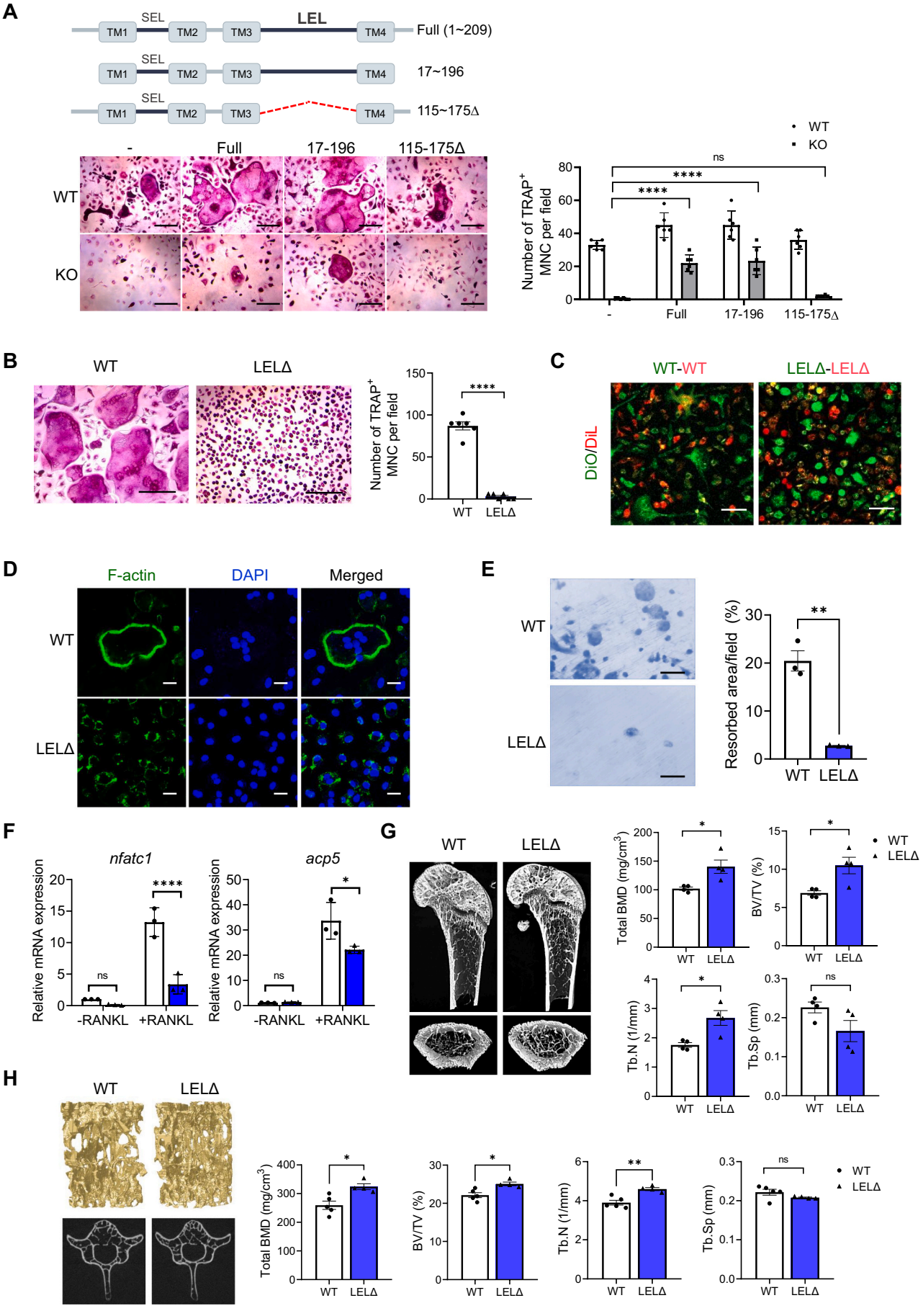

(caption on next page)

Fig. 3. The large extracellular loop (LEL) of Tm4sf19 is essential for osteoclast differentiation. (A) The structure of deletion mutant (upper panel) and BMMs isolated from WT and KO were transfected with Full, 17–196, and 115-175Δ mutants via lentiviral infection, differentiated, and then stained with TRAP (lower left panel). Scale bar, 200 μm. The number of TRAP-positive multinucleated cells were measured (lower right panel) (B) TRAP staining of differentiated osteoclasts isolated from WT and LELΔ mice. Scale bar, 200 μm. (C) Images obtained by Time-lapse microscopy during osteoclastogenesis in WT and LELΔ. Images were captured at 28 h and 8 min. Time-lapse microscopy analyses are shown in Supplementary Movies 3 and 4. Scale bar, 50 μm. (D) Representative fluorescence microscopy images of actin belts and actin rings of WT and LELΔ after osteoclast differentiation. Scale bar, 20 μm. (E) Bone resorption pit assay using mature WT and LELΔ osteoclasts using dentine discs. Blue stained structures indicate resorption pits. Scale bars; 50 μm. Resorbed area per field was analyzed. (F) Expression of osteoclast differentiation marker genes after osteoclastogenesis. (G–H) Representative μCT images of the femur or lumbar vertebrae of WT and LELΔ mice. Total BMD, BV/TV and Tb.N were analyzed with CTAn. (G) A 2 mm slice of scanned from the growth plate was selected for trabecular bone analysis in WT and LELΔ mice ($n = 4$–5). Significance was calculated by *t*-test compared to WT; $^{*}p < 0.05$. (H) Representative 3D images of vertebral trabecular bones (top) and 2D slice images (bottom). The fifth lumbar vertebra was used for analysis. Significance was calculated by *t*-test or two-way ANOVA compared to WT; $^{*}p < 0.05$, $^{**}p < 0.01$, $^{***}p < 0.001$, $^{****}p < 0.0001$, ns = no significance.

differentiation. The expression of *tm4sf19* was not detected in both undifferentiated and differentiated osteoblasts (Fig. 2H). We measured ALP activity via alkaline phosphatase staining and assessed calcium phosphate deposition via alizarin red staining and found that Tm4sf19 deficiency did not affect osteoblast differentiation and function. (Fig. 2I–J). The expression of osteoblast markers *osteocalcin* and *osteonectin*, *runx2*, a factor essential for osteoblast differentiation, and *mmp13*, a bone-associated MMP, increased when osteoblasts isolated from the mouse calvaria were differentiated, but no differences were observed between WT and KO mice (Figs. 2K and S7A). These data suggest that Tm4sf19 may not involve in osteoblast differentiation. We also investigated whether the higher trabecular bone mass in KO mice could be attributed to increased bone formation by osteoblast activation. In the femurs of 6-week-old KO mice, the expression levels of the osteoblast markers Runx2 and Osterix and the mature osteoclast marker Mmp13 were similar with WT mice (Fig. S7B). In addition, no difference of the rate of bone formation was found in WT and KO mice by measuring the number of osteocalcin-positive osteoblasts (Fig. S7C). Furthermore, PINP levels were similar in the serum of WT and KO mice at various age (Fig. S7C). These data suggest that depletion of Tm4sf19 impairs osteoclast activation but has little effect on osteoblast differentiation and function.

3.3. The large extracellular region (LEL) of Tm4sf19 is important for its function in osteoclast

To identify regions of the Tm4sf19 protein required for its function in osteoclasts, we constructed lentiviral expression vectors for full-length human Tm4sf19, $Tm4sf19_{115\text{-}175\Delta}$ in which the LEL region was removed, and $Tm4sf19_{17–196}$ with the N-terminal and C-terminal intracellular regions were removed. These constructs were transduced into BMMs isolated from WT or KO mice using lentiviral infection system. Interestingly, Tm4sf19 full-length and 17–196 rescued osteoclast multinucleation in KO BMMs. However, $Tm4sf19_{115\text{-}175\Delta}$ did not rescue the defect in osteoclast differentiation in KO BMMs (Fig. 3A). These results indicate that LEL region of Tm4sf19 is required for its function in osteoclast differentiation and the short N-terminal and C-terminal intracellular regions of Tm4sf19 do not affect the differentiation of osteoclasts.

Accordingly, we generated LEL knockout mice (LELΔ) in which the LEL region of Tm4sf19 was deleted using the CRISPR system (Fig. S8) [16]. In osteoclasts derived from WT mice, multinucleation was effectively induced, whereas in osteoclasts derived from LELΔ mice, osteoclast differentiation defined by TRAP staining was inhibited, as in $tm4sf19^{-/-}$(KO) osteoclasts (Figs. 3B and S9A). We also investigated osteoclast migration, fusion, and multinucleate formation by real-time microscopic analysis. Multinucleated osteoclast formation was observed in co-cultures of WT-founder osteoclasts and WT-follower osteoclasts, whereas multinucleated osteoclast formation was inhibited in co-cultures of LELΔ-founder osteoclasts and LELΔ-follower osteoclasts (Fig. 3C and Supplementary Movies 3, 4). Furthermore, we observed multinucleated osteoclast formation in co-culture with unlabeled-WT-founder and DiO-labeled-WT or LELΔ-follower cells, but not in mixtures of unlabeled-LELΔ-founder and DiO-labeled-LELΔ-follower cells (Fig. S9B). High concentration of M-CSF (100 ng/ml) did not complement for the multinucleation defect of LELΔ osteoclasts (Fig. S10). To determine whether the LEL region of Tm4sf19 is involved in the actin organization of osteoclasts, we examined actin belt formation using mature osteoclasts from WT and LELΔ BMMs. LELΔ osteoclasts formed only actin rings and failed to form actin belts as the case with KO osteoclasts (Fig. 3D). Bone resorption activity was also inhibited in LELΔ osteoclasts (Fig. 3E). After osteoclastogenesis, we found that the expression of osteoclast differentiation-related genes was suppressed in LELΔ osteoclasts compared to WT (Fig. 3F).

Next, we investigated whether deleting the LEL region of Tm4sf19 increases bone mass in μCT analysis. Characteristic features of bone mass, including total BMD, % BV/TV, and Tb.N, were higher and Tb.Sp. was lower in the femur and lumbar vertebrae of 12-week-old LELΔ female mice compared to WT (Fig. 3G–H). We also examined femur and lumbar trabecular bone mass in young or aged WT and LELΔ mice using μCT analysis. Interestingly, the bone mass of LELΔ mice was higher than that of WT mice. Total BMD, % BV/TV and the Tb.N of the femur and lumbar spine of LELΔ mice was higher than that of WT mice (Fig. S11A–B). Of note, % BV/TV in WT mice decreased significantly with age but did not change in KO and LELΔ mice, and the bone mass of aged KO and LELΔ mice was significantly higher than that of WT mice of the same age. (Figs. S6 and S11). These observations indicate that Tm4sf19 may be involved in bone aging, and that depletion of Tm4sf19 prevents bone mass loss during aging. As seen in KO mice, bone turnover markers in aged WT and LELΔ were not different (Fig. S11C–D). The aged KO and LELΔ mice had no physical abnormalities and their various organ weights were similar to WT mice (Fig. S12). Serum PINP1 concentrations in 12-week-old WT and LELΔ mice were similar (Fig. S13A). There were no differences in the expression of proteins associated with osteogenesis, including Runx2, Osterix, and Mmp13, observed in femurs of 6-week-old WT and LELΔ mice (Fig. S13B) and the tibia of 2–5-day-old neonatal WT and LELΔ mice (Fig. S12C). These results suggest that deficiency of the LEL region of Tm4sf19 inhibits the formation of multinucleated osteoclasts, which are important for bone resorption, and increases trabecular bone mass without any effect on osteoblast differentiation and function.

3.4. Tm4sf19 LEL fusion protein inhibits osteoclast differentiation and bone resorption

In this study, we found that osteoclast differentiation is inhibited in both KO and LELΔ osteoclasts, resulting in increased bone mass, and that the LEL region of Tm4sf19 is required for its function. These findings suggest that Tm4sf19 may be a desirable therapeutic target for bone-destroying diseases. Therefore, we generated a competitive protein inhibitor that fused the LEL region, amino acids 116–165 of mouse Tm4sf19, to an Fc protein. Prediction of the 3D structure of LEL-hIgG1 revealed the flexibility of the LEL region (Fig. 4A–B). The purified LEL-Fc fusion protein and the control hIgG1 protein showed molecular weights of 64.6 kDa and 56 kDa, respectively, when analyzed by SDS-PAGE under non-reducing conditions, and the purity of the purified Fc fusion protein was <99 % as measured by HPLC (Fig. S14A–B). We

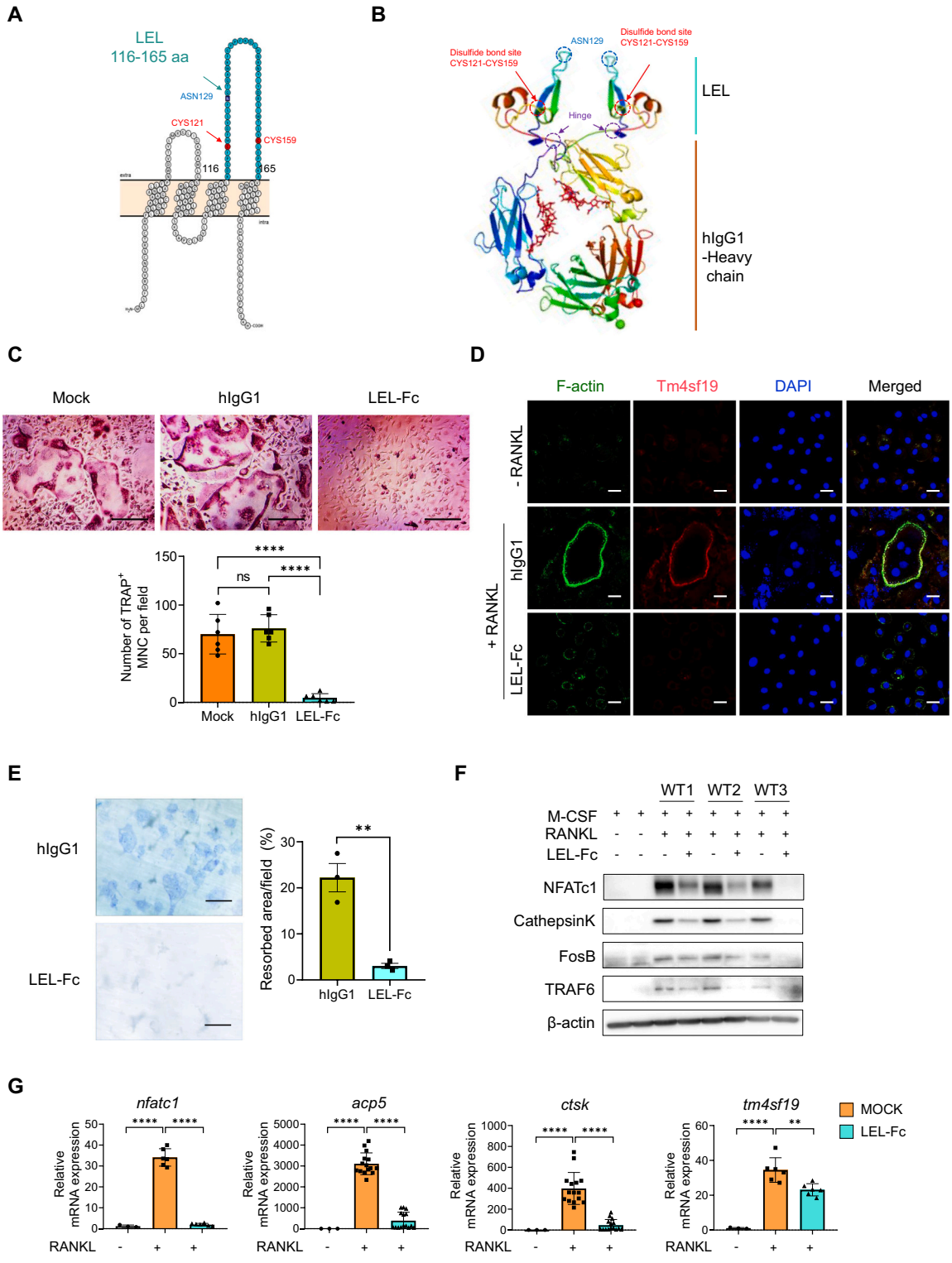

Fig. 4. Tm4sf19 LEL-Fc inhibited osteoclast differentiation. (A) Structure of Tm4sf19 LEL-Fc. The region of mouse Tm4sf19 LEL (116–165 aa) was used for the generation of LEL-Fc fusion protein. (B) 3D Structure of LEL-Fc fusion protein. Two disulfide bonding sites, N-glycosylation sites, and hinge regions are shown. (C) Representative images of osteoclast differentiation in mock, 5 μg/ml hIgG or LEL-Fc treated osteoclasts by TRAP staining. Scale bar, 200 μm. The number of multinucleated cells were counted. (D) Representative fluorescence microscopy images of actin rings and actin belts of undifferentiated and differentiated osteoclasts treated with hIgG1 or LEL-Fc. F-actin and anti-Tm4sf19 antibodies were used. Scale bar, 20 μm. (E) Representative images for resorption pit assay of hIgG1 or LEL-Fc treated osteoclasts using dentine discs. Blue stained structures indicate resorption pits. Scale bars; 50 μm. Resorbed area per field was analyzed. (F) Western blotting analysis of WT osteoclasts treated with 5 ng/ml LEL-Fc during osteoclastogenesis. The expression of proteins was examined with indicated antibody. (G) The expression of osteoclast differentiation-associated genes in LEL-Fc treated osteoclasts compared to undifferentiated osteoclast and mock. All quantitative data are shown as mean of triplicates with ±SD and the significance was analyzed by one-way ANOVA; $^{**}p < 0.01$, $^{***}p < 0.001$, $^{****}p \leq 0.0001$, ns = no significance.

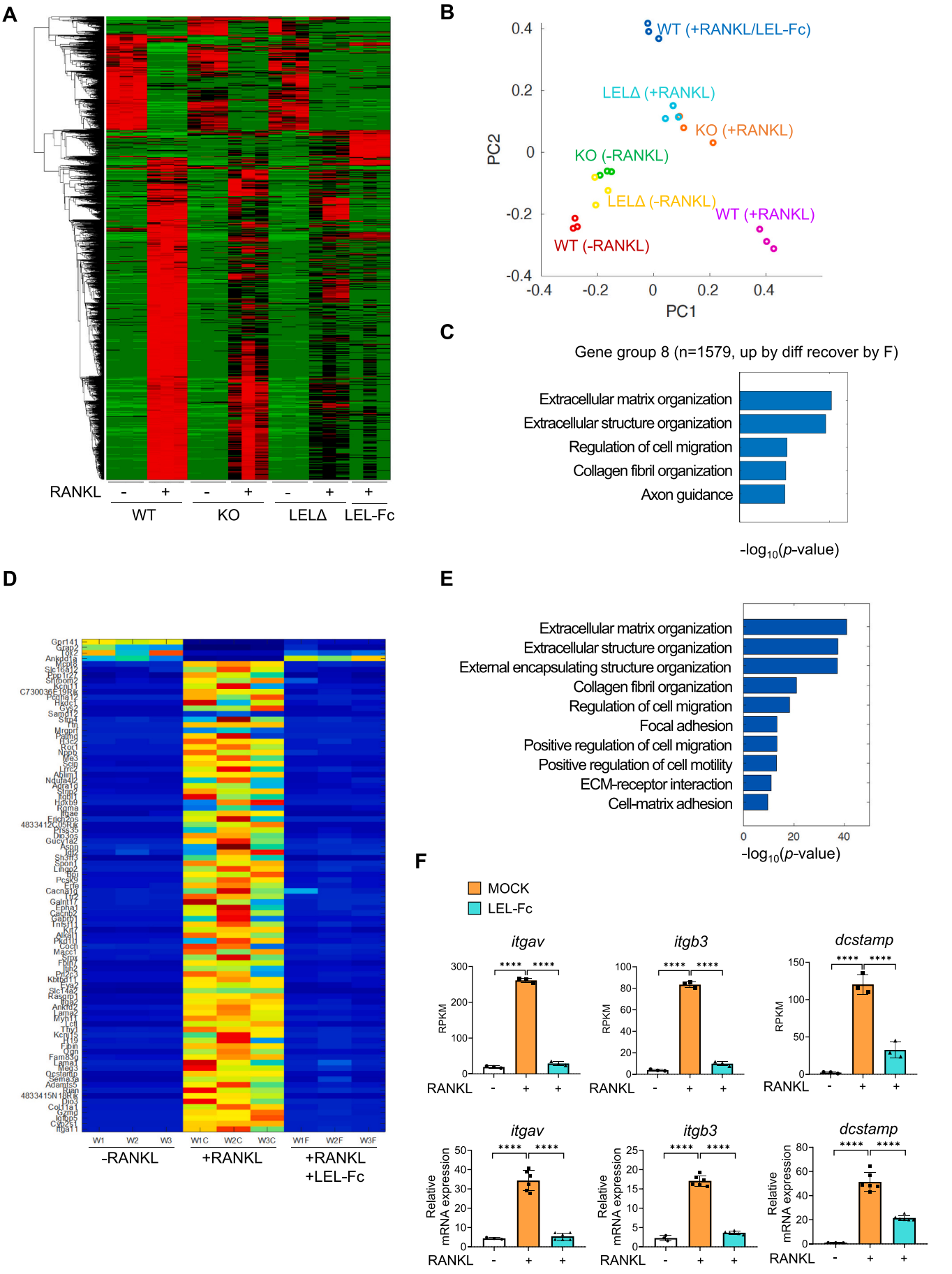

(caption on next page)

Fig. 5. RNA-sequencing analysis. (A) Heatmap plot of hierarchical clustering shows the DEGs of KO, LELΔ, and LEL-Fc treated osteoclasts compared to WT. Triplicate samples from each group were analyzed with or without RANKL induction. (B) PCA plots of each sample showed that LEL-Fc treated samples had distinct gene signatures for both WT undifferentiated and differentiated, but similar gene signatures to KO and LELΔ. (C) KEGG analysis of gene group 8, up-regulated genes by differentiation and suppressed by LEL-Fc treatment. (D–F) Gene expression signatures of LEL-Fc treatment. (D) Heatmap plot of DEGs up-regulated by differentiation but downregulated by differentiation treated with LEL-Fc and DEGs downregulated by differentiation but upregulated by differentiation treated with LEL-Fc. (E) Threshold values of Gene ontology and KEGG pathway terms associated with DEGs upregulated by differentiation but downregulated by differentiation treated with LEL-Fc. (F) Validation of target gene expression by RNA-sequencing analysis. Statistical analysis was performed with data from at least three independent experiments. Significance was calculated by one-way ANOVA; $^{****}p < 0.0001$.

identified that the expression of Tm4sf19 increases at a later stage of the osteoclast differentiation process, leading to an increased surface binding affinity of LEL-Fc in differentiated osteoclasts compared to undifferentiated osteoclasts (Fig. S14C).

First, to optimize the concentration of LEL-Fc, we performed cell proliferation assay. We found that LEL-Fc treatment in osteoclast had no effect on cell viability up to 50 μg/ml (Fig. S15A). Next, we evaluated the inhibitory effect of LEL-Fc on osteoclast maturation through serial dilutions of LEL-Fc (Fig. S15B). We found that 10 μg/ml of LEL-Fc effectively inhibited osteoclast maturation without affecting cell death (Figs. 4C and S15C). We also found that LEL-Fc treatment initiated with RANKL treatment (D0) had a better inhibitory effect on multinucleated osteoclast formation compared to the later stages (D1 or D2) of osteoclast differentiation (Fig. S16). We evaluated the effect of LEL-Fc treatment on osteoclast differentiation using hIgG1 as a control. Furthermore, actin belt formation and the osteoclastic bone resorption activity confirmed by the pit formation assay were inhibited by LEL-Fc treatment (Fig. 4D–E). During osteoclast differentiation, we found that the expression of osteoclastogenesis-related proteins NFATc1, Cathepsin K, FosB, and TRAF6 was increased by RANKL treatment but inhibited by LEL-Fc treatment (Fig. 4F). We found that the expression of genes involved in osteoclast differentiation, *nfatc1*, *acp5*, and *ctsk* was suppressed by LEL-Fc treatment after differentiation. We also found that the expression of *tm4sf19* was suppressed in response to LEL-Fc treatment in the presence of RANKL (Fig. 4G).

3.5. Transcriptome analysis showed that tm4sf19 is associated with cytoskeleton in osteoclast

Next, we characterized the genes involved in Tm4sf19-induced osteoclast multinucleation by RNA sequencing. Analysis of differentially expressed genes (DEGs) in RANKL-induced osteoclast differentiation revealed similar patterns in KO osteoclasts, LELΔ osteoclasts, and LEL-Fc-treated WT osteoclasts (Fig. 5A). In principal component analysis, RANKL-treated KO osteoclasts and LELΔ osteoclasts were positively correlated, as was the RANKL/LEL-Fc treatment group (Fig. 5B). Eight groups were identified through KEGG pathway enrichment analysis (Fig. S17A). Among them, group 8 involved in the regulation of the organization and trafficking of the extracellular matrix and extracellular structures (Figs. 5C and S17A). Furthermore, DEG analysis showed that the expression of genes whose expression was upregulated by RANKL treatment was suppressed by LEL-Fc treatment (Fig. 5D). KEGG pathway analysis revealed that Tm4sf19 is involved in extracellular structure organization, migration, and adhesion during osteoclast differentiation (Fig. 5E). We also found that the expression of osteoclast-specific genes, including genes related to osteoclast adhesion, fusion, and differentiation, was suppressed in KO, LELΔ, and LEL-Fc-treated osteoclasts compared to WT osteoclasts after osteoclast differentiation (Figs. S17B and S18). Next, we confirmed the expression of osteoclast differentiation-related marker genes obtained by RNA sequencing analysis. We found that the expression of *itgav*, *itgb3*, *dcstamp*, and *tm4sf19* increased after osteoclast differentiation, but their expression was reduced by LEL-Fc treatment (Figs. 5F and S18).

3.6. The LEL region of Tm4sf19 plays an important role in binding to the integrin αvβ3

Tetraspanins are a class of essential transmembrane proteins that regulate a variety of cellular processes. Members of the tetraspanin family are involved in intracellular or intercellular interactions through homodimer and dimer formation. The LELs of tetraspanins are primarily involved in these interactions [20,21]. By immunoprecipitation, we confirmed that full-length Tm4sf19 binds to LELΔ. However, a $Tm4sf19_{94–196Δ}$ failed to bind full-length Tm4sf19 (Fig. 6A–B). Interestingly, Tm4sf19 mutants deleted from TM3 to the N-terminal half of TM4 (94-186Δ) bound full-length Tm4sf19, whereas Tm4sf19 mutants deleted from TM3 to the entire TM4 did not interact with full-length Tm4sf19. These results suggest that 10 amino acids in the C-terminal half of TM4 may be essential for homodimerization of Tm4sf19 (Fig. 6B). We confirmed that $Tm4sf19_{120–169}$ interacts with the full-length Tm4sf19, whereas it does not interact with the $Tm4sf19_{115\text{-}175Δ}$ or $Tm4sf19_{94–196Δ}$ (Fig. 6C). Furthermore, we demonstrated that a Tm4sf19 deletion mutant expressing only the 94–196 amino acid (a.a.) region can interact with full-length Tm4sf19 (Fig. 6D). We also found that the mouse Tm4sf19-LEL (116–165 a.a.) region, which shows high homology to the human Tm4sf19-LEL (120–169 a.a.) region, interacts with full-length mouse Tm4sf19 (Fig. S19A).

Tetraspanins can interact laterally with other tetraspanins or partner proteins to form tetraspanin-rich microdomains (TEMs) on the cell surface [22]. To investigate whether Tm4sf19 binds and oligomerizes with each other to form functional sites, the TEMs, we examined Tm4sf19 oligomerization upon transient or stable expression of Tm4sf19 in CHO-K1 cells. Tm4sf19 monomers were observed at around 30 kDa, slightly larger due to N-glycosylation, while multimers were observed to increase in a dose-dependent manner above 55 kDa (Fig. S19B). Next, we investigated which regions of Tm4sf19 were important for oligomerization of Tm4sf19. Full-length Tm4sf19 mainly formed multimers, whereas the 115-175Δ and 94-196Δ mutants mainly formed monomers (Fig. 6E). These results suggest that the TM3-4 and LEL regions of Tm4sf19 are involved in Tm4sf19 homodimer formation.

Furthermore, RNA sequencing revealed that Tm4sf19 is involved in the organization of extracellular structures during osteoclast differentiation. Therefore, we investigated the association of Tm4sf19 with integrin αvβ3, which regulate the cytoplasmic structure of osteoclasts for adhesion. Full-length Tm4sf19 was found to interact with integrins αv and β3, but Tm4sf19 lacking the LEL region did not form complexes with these integrins (Fig. 6F–H). We also found an interaction between the LEL region of mouse Tm4sf19 and αv integrin or β3 integrin (Figs. 6I and S20). In stable full-length Tm4sf19-expressing osteoclasts, the interaction between Tm4sf19 and αv integrin was visualized as a fluorescent signal by Duolink® proximity binding assay, whereas in $Tm4sf19_{115\text{-}175Δ}$-expressing osteoclasts, no interaction between integrin αv and $Tm4sf19_{115\text{-}175Δ}$ was observed (Fig. S21). In addition, endogenous interaction of Tm4sf19 and integrin αv was confirmed in the presence or absence of vitronectin, which induces integrin-related signaling and cell adhesion (Fig. 6J). However, deficiency of Tm4sf19 had no effect on the expression integrin αvβ3 in mice (Fig. S22).

Cytoskeletal remodeling is responsible for osteoclast migration, fusion, and bone resorption [15]. Osteoclasts attach to bone through actin-related adhesions that are regulated by M-CSF and integrin signaling [23–25]. When M-CSF and integrin signaling are impaired, the

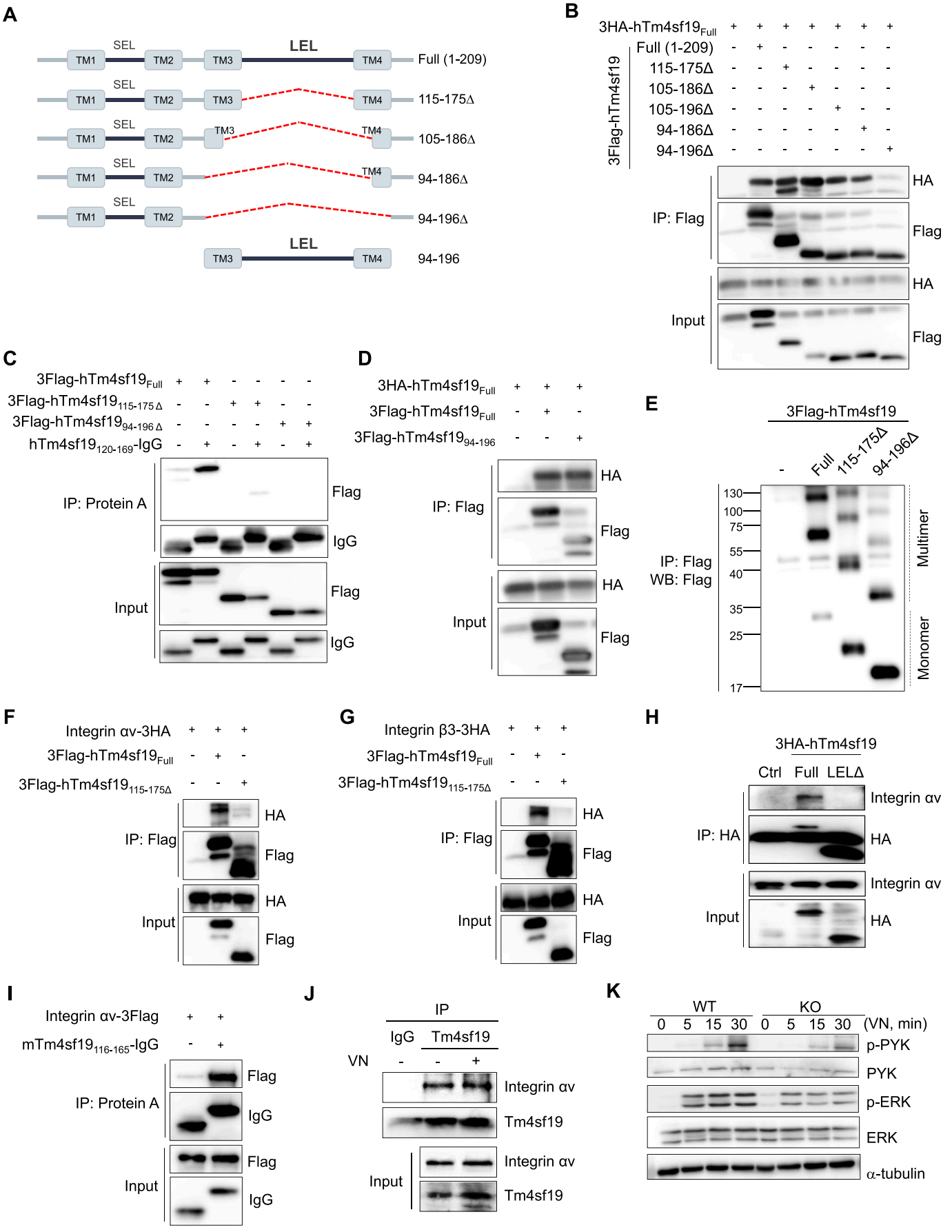

(caption on next page)

Fig. 6. Tm4sf19 associated with integrin αvβ3. (A) Map of deletion mutants (right) of Tm4sf19. Four transmembranes (TM1–4), a small extracellular loop (SEL), a large extracellular loop (LEL) and two intracellular regions are presented. (B) Immunoprecipitation results of Tm4sf19 with deletion mutants of Tm4sf19. 3HA-tagged full length and 3Flag-tagged full- or deletion mutants of Tm4sf19 were co-transfected in 293T cells. Cell lysates were immunoprecipitated with anti-Flag antibody. (C) Interaction of $hTm4sf19_{120–169}$ with full or deletion mutants of human Tm4sf19 in 293T. Immunoprecipitation was performed with Protein A agarose beads. (D) Immunoprecipitation results of Tm4sf19 with deletion mutant, only expressed 94–196 amino acid of hTm4sf19. 3HA-tagged $hTm4sf19_{Full}$ was co-transfected with either 3Flag-tagged $hTm4sf19_{Full}$ or $hTm4sf19_{94–196}$ deletion mutant in 293T. Immunoprecipitation was performed with anti-Flag antibody. (E) Oligomerization of deletion mutants. 3Flag tagged at the N-terminus of full, LEL deletion (115-175Δ) mutant and TM 3-LEL-TM 4 deletion (94-196Δ) mutant of Tm4sf19 were transiently transfected in CHO-K1 cells. Immunoprecipitation was performed with anti-Flag antibody. (F–G) Immunoprecipitation results of integrin αv or β3 and $hTm4sf19_{Full}$ and $hTm4sf19_{115\text{-}175\Delta}$ mutant. 3HA tagged at the C-terminus of integrin αv or β3 and 3Flag tagged $hTm4sf19_{Full}$ or $hTm4sf19_{115\text{-}175\Delta}$ mutant were co-transfected in 293T cells and the interaction was examined by immunoprecipitation with anti-Flag antibody. (H) Endogenous interaction of Tm4sf19 with integrin αv. Stably Tm4sf19 expressed Raw 264.7 cells were differentiated in the presence of RANKL. Immunoprecipitation was performed with anti-HA antibody. (I) Interactions between mouse $Tm4sf19_{116–165}$ and integrin αv. The constructs were co-transfected in 293T and cell lysates were pulled down with Protein A-agarose beads. (J) Endogenous interaction of Tm4sf19 and integrin αv on differentiated Raw264.7 cell with or without vitronectin-based cell adhesion. (K) Western blot results of WT and KO mature osteoclasts were plated on vitronectin-coated plates for the indicated times to evaluate integrin αvβ3-related signals.

number and size of osteoclast fusions decrease [26–28]. In this study, we found that the expression of phospho-ERK induced by M-CSF in KO BMMs was comparable to WT BMMs (Fig. S23A). In addition, there were no differences in phospho-p65 and phospho-p38 between WT and KO BMMs induced by RANKL (Fig. S23B). These data indicated that the inhibition of osteoclast differentiation in KO osteoclasts was independent of the M-CSF and RANKL signaling pathways. However, the reduction of vitronectin-induced PYK2 tyrosine phosphorylation and ERK phosphorylation in KO osteoclasts compared to WT osteoclasts suggests that Tm4sf19 plays an important role in integrin αvβ3 signaling during osteoclast multinucleation (Fig. 6K) [29–32]. Furthermore, examination of ERK phosphorylation by M-CSF signaling in WT and LELΔ osteoclasts showed no difference, but vitronectin-induced phosphorylation of Pyk2 and ERK was significantly reduced in LELΔ osteoclasts (Fig. S24). These results indicate that the LEL region of Tm4sf19 directly binds to integrin αvβ3 and regulates integrin αvβ3 signaling in osteoclast differentiation (Figs. 6F–K and S24).

3.7. *Tm4sf19 LEL-Fc protected from bone loss in mouse model of osteoporosis*

Since Tm4sf19 binds to integrin αvβ3 via LEL to regulate integrin αvβ3 signaling, we investigated whether the LEL-Fc protein also binds to integrin αvβ3. As expected, the *in vitro* binding of LEL-Fc to recombinant integrin αvβ3 protein was confirmed by ELISA assay (Fig. 7A). In addition, we also confirmed LEL-Fc self-binding by ELISA assay (Fig. 7B). We also observed that LEL-Fc inhibited the interaction of integrin αv with Tm4sf19 or the dimerization of Tm4sf19 with Tm4sf19 (Fig. 7C–D). These data suggest that LEL-Fc may inhibit osteoclast differentiation by interfering with the binding of Tm4sf19 and its binding partners at the plasma membrane.

It has been studied therapeutic effect of Fc-fusion protein including RANK-Fc fusion on bone disease. Having established that LEL-Fc treatment inhibits osteoclast differentiation, we investigated the effect of LEL-Fc treatment on osteoporosis in an *in vivo* mouse model. Concentration showing the effect of preventing bone destruction by murine RANK-Fc fusion protein was used [33]. The ovariectomized mouse group showed dramatic trabecular bone loss in the femur compared to the sham group, but treatment with LEL-Fc significantly rescued the osteoporotic phenotype in a dose-dependent manner (Fig. 7E). In the osteoporotic mouse model, total BMD, % BV/TV, and Tb.N were higher and Tb.Sp was lower in the LEL-Fc treatment group compared to the mock control (Fig. 7F). Histologic analysis revealed higher trabecular bone mass but lower TRAP intensity per bone surface in the 5 mg/kg and 10 mg/kg LEL-Fc treatment groups compared to the mock control (Fig. 7G). These results suggest that LEL-Fc is a potential treatment for osteoclast-related diseases caused by osteoclast hyperactivation.

4. Discussion

Multinucleated osteoclasts are characterized by their unique ability to resorb large amounts of bone. Osteoclasts have been the direct target of several therapeutic agents to prevent bone loss in various bone diseases via inhibiting bone resorption [2,12,34–36]. In this study, we found BMMs from Tm4sf19 KO and LELΔ had defect in osteoclast differentiation and bone resorption activity (Figs. 2A–D and 3B–F). In addition, Tm4sf19 LEL-fusion protein effectively inhibited osteoclast differentiation and bone resorption (Fig. 4C–G). The LEL region of tetraspanins is known to play a pivotal role in tetraspanin network formation. The LEL is categorized into conserved and variable domains. The diversity of the variable domains is speculated to determine the interaction partners selected for network formation [37–41]. A previous report showed that solution NMR studies of LEL revealed significant conformational flexibility in this region [42], suggesting that the LEL region is an important mediator of tetraspanin interactions. In this regard, it is interesting to note that the Tm4sf19 LEL-Fc fusion protein, a competitive inhibitor of Tm4sf19, can inhibit homozygous interactions of Tm4sf19 as well as lateral interactions in *cis* with other tetraspanins and partner proteins involved in tetraspanin web construction. We demonstrated that the Tm4sf19 LEL-Fc fusion protein effectively suppressed osteoclast-associated bone disease by blocking osteoclast function and inhibiting the interaction of Tm4sf19 with its binding partners (Fig. 7). Administration of LEL-Fc did not change body weight and liver and spleen weight (Fig. S25A–B). Histopathological analysis of liver and spleen also showed that LEL-Fc had no adverse effect (Fig. S25C). We also found that LEL-Fc treatment did not change immune cell distribution (Fig. S26). In addition, administration LEL-Fc on 8-week-old mice for 9 weeks had no effect on the growth plates (Fig. S27). These data suggest that administration of LEL-Fc may not have any side effects in mice.

Interestingly, although osteoclast differentiation was inhibited in KO BMM compared to WT BMM, severe osteopetrosis as in $Tnfsf11^{-/-}$, $Csf1r^{-/-}$, $Src^{-/-}$ and $Nfatc1^{-/-}$ mice, which are known to affect trabecular bone mass, was not observed in $tm4sf19^{-/-}$ mice [43–46]. In some cases, the skeletal parameters of the knockout mice did not always match the results of *in vitro* osteoclast differentiation and bone resorption activity. As seen in $tm4sf19^{-/-}$ mice, osteoclast maturation was also significantly inhibited in $Atp6v0d2^{-/-}$ BMMs, but no severe osteopetrosis was seen in $Atp6v0d2^{-/-}$ mice [34,47,48]. Furthermore, $DC\text{-}STAMP^{-/-}$ mice showed increased bone mass and mild osteopetrosis despite complete blockage of osteoclast intercellular fusion, resulting in defective multinucleated osteoclast formation and inhibited bone resorption activity in pit formation assays [49–51]. Furthermore, BMMs from $OC\text{-}STAMP^{-/-}$ mice formed only mononuclear osteoclasts, failed to form multinucleated osteoclasts, and significantly reduced bone resorption in pit forming assay, whereas $OC\text{-}STAMP^{-/-}$ mice showed a normal skeletal phenotype [2,52–56].

The cytoskeleton is composed of actin filaments, microtubules, and intermediate filaments and is involved in cell shape, cell motility, cell adhesion, migration, and polarity maintenance. In particular, the cytoskeleton of osteoclasts is essential for their bone resorption activity. The attachment of osteoclasts to the bone surface is accomplished by actin

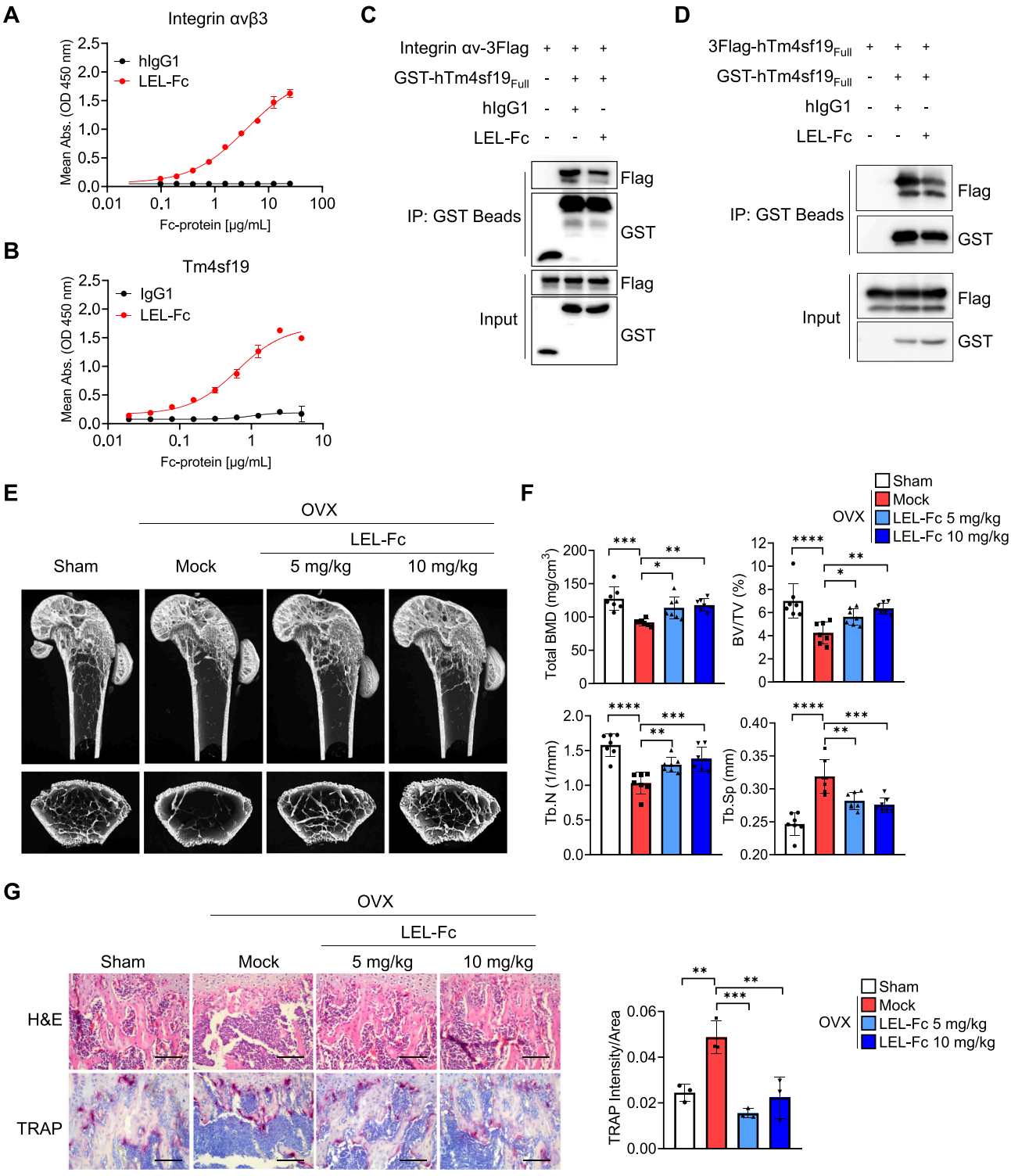

Fig. 7. Tm4sf19 LEL-Fc showed therapeutic effect on osteoporosis mouse model. (A–B) Enzyme-linked immunosorbent assay (ELISA) of integrin αvβ3, and Tm4sf19 with LEL-Fc fusion protein. (A) Binding affinity was measured with various concentrations of hIgG1 or LEL-Fc and 1 μg/ml of recombinant integrin αvβ3. (B) LEL-Fc was used for Tm4sf19 and LEL-Fc interaction. (C-D) Immunoprecipitation results of Tm4sf19 and integrin αv or Tm4sf19 with hIgG1 or LEL-Fc treatment. Immunoprecipitation was performed with glutathione Sepharose beads and Western blotting was conducted with indicated antibodies. (E–F) Bone analysis was performed with femurs of sham and ovariectomized mice treated with 5 mg/kg or 10 mg/kg LEL-Fc ($n = 7$). (E) Representative μCT images, and (F) trabecular bone analysis. Parameters; total bone mineral density (BMD, mg/cm^3), bone volume per trabecular volume (BV/TV), trabecular numbers (Tb.N), and trabecular separation (Tb.Sp). (G) Histological analysis of femurs in H&E (upper) and TRAP staining (lower). Scale bar indicates 100 μm. Relative TRAP intensity per area was measured. All the quantitative data were presented by meat with ±SD and the significance was calculated by one-way ANOVA; *$p < 0.05$, **p < 0.01, ***p < 0.001, ****p < 0.0001.

belts composed of packs of podosomes, and integrin αvβ3 plays a key role in this process. We found that Tm4sf19 interacts with integrin αv and integrin β3, transmembrane proteins of osteoclasts. The LEL region of Tm4sf19 was found to be involved in their interactions (Fig. 6F–I). When the formation of actin belt is disrupted, bone resorption is impaired. In this study, we demonstrated that Tm4sf19 co-localized with F-actin in the actin belt of osteoclasts (Fig. 1E) and that KO and LELΔ osteoclasts fail to form actin belts and their bone resorption activity is inhibited (Figs. 2C–D and 3D–E), indicating that Tm4sf19 plays an important role in the cytoskeleton rearrangement. Interestingly, the Tm4sf19 LEL-Fc fusion protein also inhibited actin belt formation, suggesting that the LEL domain of Tm4sf19 is an important domain for Tm4sf19 activity in regulating actin belt formation and bone resorption (Fig. 4D–E).

Osteoclast multinucleation occurs by intercellular fusion through reorganization of the cytoskeleton. In this dynamic process, various membrane-associated proteins are recruited on to the protein cluster by the membrane organizer. Tetraspanin-enriched microdomains (TEM) formed by multiple interactions of tetraspanin with other proteins in the cell membrane are considered to serve as membrane organizers [6,57,58]. The LEL region of Tm4sf19 has a highly conserved cysteine motif that is characteristic of tetraspanins. We found that Tm4sf19 not only binds to each other, but also to another tetraspanin family members (data not shown) and to osteoclast transmembrane proteins such as integrin αv and integrin β3 (Fig. 6B–J). It is possible that Tm4sf19 may also bind to other integrin families and regulates other cellular processes. These data suggest that Tm4sf19 may contribute to form microdomains at the plasma membrane through intramolecular and intermolecular interactions during osteoclastogenesis.

5. Conclusion

Abnormal osteoclast activation causes many types of bone diseases. Modulation of osteoclast activity is a good strategy for the treatment of osteoclast-associated bone diseases. In this study, we demonstrated that Tm4sf19 regulates osteoclast differentiation and the large extracellular loop (LEL) of Tm4sf19 is responsible for its function. We generated a LEL-Fc fusion protein and confirmed its protective effect against bone loss in an osteoporosis model. We confirmed that LEL-Fc didn't show any side effect in mice. This study provides information to understand the role of Tm4sf19 in osteoclasts and suggests that Tm4sf19 LEL-Fc is a potential therapeutic for osteoclast-associated bone diseases.

Supplementary data to this article can be found online at https://doi.org/10.1016/j.metabol.2023.155746.

CRediT authorship contribution statement

Sujin Park: Conceptualization, Investigation, Supervision, Validation, Writing – original draft, Writing – review & editing. **Jin Sun Heo:** Formal analysis, Investigation, Methodology. **Seiya Mizuno:** Investigation, Resources. **Minwoo Kim:** Investigation, Resources. **Haein An:** Formal analysis, Investigation, Visualization, Writing – original draft. **Eunji Hong:** Formal analysis, Investigation, Visualization, Writing – original draft. **Min Gi Kang:** Investigation. **Junil Kim:** Formal analysis. **Rebecca Yun:** Investigation. **Hyeyeon Park:** Investigation. **Eun Hye Noh:** Investigation. **Min Jung Lee:** Visualization. **Kwiyeom Yoon:** Investigation. **Pyunggang Kim:** Investigation. **Minjung Son:** Investigation. **Kyoungwha Pang:** Investigation. **Jihee Lee:** Investigation. **Jinah Park:** Investigation. **Akira Ooshima:** Formal analysis. **Tae-Jin Kim:** Investigation. **Je Yeon Park:** Investigation. **Kyung-Min Yang:** Investigation. **Seung-Jae Myung:** Formal analysis. **Hyun Bae:** Writing – review & editing. **Kyung-Mi Lee:** Writing – review & editing. **John Letterio:** Writing – review & editing. **Seok Hee Park:** Writing – review & editing. **Satoru Takahashi:** Writing – review & editing. **Seong-Jin Kim:** Conceptualization, Supervision, Writing – original draft, Writing – review & editing.

Declaration of competing interest

S.J.K. is a founder of Medpacto, and a co-founder of Theragen, Celloram, and Medpacto Theraeputics and serves on the boards of directors at Medpacto, Theragen, Celloram, and Medpacto Therapeutics. J.L. is a co-founder of Celloram and serves on the boards of directors at Celloram. J.L. and H.B. are members of the clinical advisory boards of Medpacto. M.W.K., E.H.N., M.J.L., B.K.K., K.Y., and K.M.Y. are employees of Medpacto. The GILO Foundation has received research support from Medpacto. The other authors declare no competing interests.

Acknowledgments

This research was in part supported by Korea Drug Development Fund funded by Ministry of Science and ICT, Ministry of Trade, Industry, and Energy, and Ministry of Health and Welfare (RS-2023-00282595, Republic of Korea).

References

[1] Kim JM, Lin C, Stavre Z, Greenblatt MB, Shim JH. Osteoblast-osteoclast communication and bone homeostasis. Cells 2020:9.
[2] Kodama J, Kaito T. Osteoclast multinucleation: review of current literature. Int J Mol Sci 2020:21.
[3] Ng AY, Tu C, Shen S, Xu D, Oursler MJ, Qu J, et al. Comparative characterization of osteoclasts derived from murine bone marrow macrophages and RAW 264.7 cells using quantitative proteomics. JBMR Plus 2018;2:328–40.
[4] Lampiasi N, Russo R, Kireev I, Strelkova O, Zhironkina O, Zito F. Osteoclasts differentiation from murine RAW 264.7 cells stimulated by RANKL: timing and behavior. Biology (Basel) 2021:10.
[5] Gielen E, Dupont J, Dejaeger M, Laurent MR. Sarcopenia, osteoporosis and frailty. Metabolism 2023;145:155638.
[6] van Deventer S, Arp AB, van Spriel AB. Dynamic plasma membrane organization: a complex symphony. Trends Cell Biol 2021;31:119–29.
[7] Ishii M, Iwai K, Koike M, Ohshima S, Kudo-Tanaka E, Ishii T, et al. RANKL-induced expression of tetraspanin CD9 in lipid raft membrane microdomain is essential for cell fusion during osteoclastogenesis. J Bone Miner Res 2006;21:965–76.
[8] Kim M, Lin J, Huh JE, Park JH, Go M, Lee H, et al. Tetraspanin 7 regulates osteoclast function through association with the RANK/alphavbeta3 integrin complex. J Cell Physiol 2022;237:846–55.
[9] Takeda Y, Tachibana I, Miyado K, Kobayashi M, Miyazaki T, Funakoshi T, et al. Tetraspanins CD9 and CD81 function to prevent the fusion of mononuclear phagocytes. J Cell Biol 2003;161:945–56.
[10] Ding L, Li LM, Hu B, Wang JL, Lu YB, Zhang RY, et al. TM4SF19 aggravates LPS-induced attenuation of vascular endothelial cell adherens junctions by suppressing VE-cadherin expression. Biochem Biophys Res Commun 2020;533:1204–11.
[11] Ahmadzadeh K, Vanoppen M, Rose CD, Matthys P, Wouters CH. Multinucleated giant cells: current insights in phenotype, biological activities, and mechanism of formation. Front Cell Dev Biol 2022;10:873226.
[12] Blangy A, Bompard G, Guerit D, Marie P, Maurin J, Morel A, et al. The osteoclast cytoskeleton - current understanding and therapeutic perspectives for osteoporosis. J Cell Sci 2020;133.
[13] Wang Y, Brooks PJ, Jang JJ, Silver AS, Arora PD, McCulloch CA, et al. Role of actin filaments in fusopod formation and osteoclastogenesis. Biochim Biophys Acta 2015;1853:1715–24.
[14] van den Dries K, Linder S, Maridonneau-Parini I, Poincloux R. Probing the mechanical landscape - new insights into podosome architecture and mechanics. J Cell Sci 2019;132.
[15] Kloc M, Subuddhi A, Uosef A, Kubiak JZ, Ghobrial RM. Monocyte-macrophage lineage cell fusion. Int J Mol Sci 2022;23.
[16] Sato Y, Tsukaguchi H, Morita H, Higasa K, Tran MTN, Hamada M, et al. A mutation in transcription factor MAFB causes focal segmental glomerulosclerosis with Duane retraction syndrome. Kidney Int 2018;94:396–407.
[17] Levaot N, Ottolenghi A, Mann M, Guterman-Ram G, Kam Z, Geiger B. Osteoclast fusion is initiated by a small subset of RANKL-stimulated monocyte progenitors, which can fuse to RANKL-unstimulated progenitors. Bone 2015;79:21–8.
[18] Yi YW, Lee JH, Kim SY, Pack CG, Ha DH, Park SR, et al. Advances in analysis of biodistribution of exosomes by molecular imaging. Int J Mol Sci 2020;21.
[19] Moon H, Sultana T, Lee J, Huh J, Lee HD, Choi MS. Biomimetic lipid-fluorescein probe for cellular bioimaging. Front Chem 2023;11:1151526.
[20] van Deventer SJ, Dunlock VE, van Spriel AB. Molecular interactions shaping the tetraspanin web. Biochem Soc Trans 2017;45:741–50.
[21] Kovalenko OV, Metcalf DG, DeGrado WF, Hemler ME. Structural organization and interactions of transmembrane domains in tetraspanin proteins. BMC Struct Biol 2005;5:11.
[22] Zou F, Wang X, Han X, Rothschild G, Zheng SG, Basu U, et al. Expression and function of tetraspanins and their interacting partners in B cells. Front Immunol 2018;9:1606.
[23] Huveneers S, Danen EH. Adhesion signaling - crosstalk between integrins, Src and Rho. J Cell Sci 2009;122:1059–69.

[24] Kim JM, Lee K, Jeong D. Selective regulation of osteoclast adhesion and spreading by PLCgamma/PKCalpha-PKCdelta/RhoA-Rac1 signaling. BMB Rep 2018;51:230–5.
[25] Anwar A, Sapra L, Gupta N, Ojha RP, Verma B, Srivastava RK. Fine-tuning osteoclastogenesis: an insight into the cellular and molecular regulation of osteoclastogenesis. J Cell Physiol 2023;238:1431–64.
[26] Nakamura I, Duong LT, Rodan SB, Rodan GA. Involvement of alpha(v)beta3 integrins in osteoclast function. J Bone Miner Metab 2007;25:337–44.
[27] McHugh KP, Hodivala-Dilke K, Zheng MH, Namba N, Lam J, Novack D, et al. Mice lacking beta3 integrins are osteosclerotic because of dysfunctional osteoclasts. J Clin Invest 2000;105:433–40.
[28] Zur Y, Rosenfeld L, Keshelman CA, Dalal N, Guterman-Ram G, Orenbuch A, et al. A dual-specific macrophage colony-stimulating factor antagonist of c-FMS and alphavbeta3 integrin for osteoporosis therapy. PLoS Biol 2018;16:e2002979.
[29] Roberts MS, Woods AJ, Shaw PE, Norman JC. ERK1 associates with alpha(v)beta 3 integrin and regulates cell spreading on vitronectin. J Biol Chem 2003;278:1975–85.
[30] Faccio R, Takeshita S, Zallone A, Ross FP, Teitelbaum SL. c-Fms and the alphavbeta3 integrin collaborate during osteoclast differentiation. J Clin Invest 2003;111:749–58.
[31] Jung YK, Jin JS, Jeong JH, Kim HN, Park NR, Choi JY. DICAM, a novel dual immunoglobulin domain containing cell adhesion molecule interacts with alphavbeta3 integrin. J Cell Physiol 2008;216:603–14.
[32] Kim H, Wrann CD, Jedrychowski M, Vidoni S, Kitase Y, Nagano K, et al. Irisin mediates effects on bone and fat via alphaV integrin receptors. Cell 2018;175:1756–68 [e17].
[33] Aghaloo TL, Cheong S, Bezouglaia O, Kostenuik P, Atti E, Dry SM, et al. RANKL inhibitors induce osteonecrosis of the jaw in mice with periapical disease. J Bone Miner Res 2014;29:843–54.
[34] Bi H, Chen X, Gao S, Yu X, Xiao J, Zhang B, et al. Key triggers of osteoclast-related diseases and available strategies for targeted therapies: a review. Front Med (Lausanne) 2017;4:234.
[35] Nedeva IR, Vitale M, Elson A, Hoyland JA, Bella J. Role of OSCAR signaling in osteoclastogenesis and bone disease. Front Cell Dev Biol 2021;9:641162.
[36] Makras P, Delaroudis S, Anastasilakis AD. Novel therapies for osteoporosis. Metabolism 2015;64:1199–214.
[37] Stipp CS, Kolesnikova TV, Hemler ME. Functional domains in tetraspanin proteins. Trends Biochem Sci 2003;28:106–12.
[38] Dharan R, Goren S, Cheppali SK, Shendrik P, Brand G, Vaknin A, et al. Transmembrane proteins tetraspanin 4 and CD9 sense membrane curvature. Proc Natl Acad Sci U S A 2022;119:e2208993119.
[39] Ivanusic D, Madela K, Bannert N, Denner J. The large extracellular loop of CD63 interacts with gp41 of HIV-1 and is essential for establishing the virological synapse. Sci Rep 2021;11:10011.
[40] Lipper CH, Gabriel KH, Seegar TCM, Durr KL, Tomlinson MG, Blacklow SC. Crystal structure of the Tspan15 LEL domain reveals a conserved ADAM10 binding site. Structure 2022;30:206–14 [e4].
[41] Kumar A, Hossain RA, Yost SA, Bu W, Wang Y, Dearborn AD, et al. Structural insights into hepatitis C virus receptor binding and entry. Nature 2021;598:521–5.
[42] Rajesh S, Sridhar P, Tews BA, Feneant L, Cocquerel L, Ward DG, et al. Structural basis of ligand interactions of the large extracellular domain of tetraspanin CD81. J Virol 2012;86:9606–16.
[43] Lowe C, Yoneda T, Boyce BF, Chen H, Mundy GR, Soriano P. Osteopetrosis in Src-deficient mice is due to an autonomous defect of osteoclasts. Proc Natl Acad Sci U S A 1993;90:4485–9.
[44] Dougall WC, Glaccum M, Charrier K, Rohrbach K, Brasel K, De Smedt T, et al. RANK is essential for osteoclast and lymph node development. Genes Dev 1999;13:2412–24.
[45] Aliprantis AO, Ueki Y, Sulyanto R, Park A, Sigrist KS, Sharma SM, et al. NFATc1 in mice represses osteoprotegerin during osteoclastogenesis and dissociates systemic osteopenia from inflammation in cherubism. J Clin Invest 2008;118:3775–89.
[46] Dai XM, Ryan GR, Hapel AJ, Dominguez MG, Russell RG, Kapp S, et al. Targeted disruption of the mouse colony-stimulating factor 1 receptor gene results in osteopetrosis, mononuclear phagocyte deficiency, increased primitive progenitor cell frequencies, and reproductive defects. Blood 2002;99:111–20.
[47] Lee SH, Rho J, Jeong D, Sul JY, Kim T, Kim N, et al. V-ATPase V0 subunit d2-deficient mice exhibit impaired osteoclast fusion and increased bone formation. Nat Med 2006;12:1403–9.
[48] Kim K, Lee SH, Ha Kim J, Choi Y, Kim N. NFATc1 induces osteoclast fusion via up-regulation of Atp6v0d2 and the dendritic cell-specific transmembrane protein (DC-STAMP). Mol Endocrinol 2008;22:176–85.
[49] Yagi M, Miyamoto T, Sawatani Y, Iwamoto K, Hosogane N, Fujita N, et al. DC-STAMP is essential for cell-cell fusion in osteoclasts and foreign body giant cells. J Exp Med 2005;202:345–51.
[50] Kukita T, Wada N, Kukita A, Kakimoto T, Sandra F, Toh K, et al. RANKL-induced DC-STAMP is essential for osteoclastogenesis. J Exp Med 2004;200:941–6.
[51] Soe K. Osteoclast fusion: physiological regulation of multinucleation through heterogeneity-potential implications for drug sensitivity. Int J Mol Sci 2020;21.
[52] Yang M, Birnbaum MJ, MacKay CA, Mason-Savas A, Thompson B, Odgren PR. Osteoclast stimulatory transmembrane protein (OC-STAMP), a novel protein induced by RANKL that promotes osteoclast differentiation. J Cell Physiol 2008;215:497–505.
[53] Miyamoto H, Suzuki T, Miyauchi Y, Iwasaki R, Kobayashi T, Sato Y, et al. Osteoclast stimulatory transmembrane protein and dendritic cell-specific transmembrane protein cooperatively modulate cell-cell fusion to form osteoclasts and foreign body giant cells. J Bone Miner Res 2012;27:1289–97.
[54] Khan UA, Hashimi SM, Bakr MM, Forwood MR, Morrison NA. Foreign body giant cells and osteoclasts are TRAP positive, have podosome-belts and both require OC-STAMP for cell fusion. J Cell Biochem 2013;114:1772–8.
[55] Witwicka H, Hwang SY, Reyes-Gutierrez P, Jia H, Odgren PE, Donahue LR, et al. Studies of OC-STAMP in osteoclast fusion: a new knockout mouse model, rescue of cell fusion, and transmembrane topology. PloS One 2015;10:e0128275.
[56] Ishii T, Ruiz-Torruella M, Ikeda A, Shindo S, Movila A, Mawardi H, et al. OC-STAMP promotes osteoclast fusion for pathogenic bone resorption in periodontitis via up-regulation of permissive fusogen CD9. FASEB J 2018;32:4016–30.
[57] Yanez-Mo M, Barreiro O, Gordon-Alonso M, Sala-Valdes M, Sanchez-Madrid F. Tetraspanin-enriched microdomains: a functional unit in cell plasma membranes. Trends Cell Biol 2009;19:434–46.
[58] Rubinstein E. The complexity of tetraspanins. Biochem Soc Trans 2011;39:501–5.